Off-axis tilt elimination in digital holographic microscopy by self-hologram rotation: applications in surface metrology

D. G. A. Ibrahim

Engineering and Surface Metrology Laboratory, National Institute of Standards (NIS),

Corresponding Author E-mail: dahi.abdelsalam@nis.sci.eg

Article Type: Research article.

Received on 24 May 2022, Accepted on 14 August 2022

Abstract:

Off-axis tilt in digital holographic microscopy is an obstacle to perfect measurement. The tilt is induced by the off-axis angle geometry between the object wave and the reference wave of the interferometer. This study uses a compensation method based on self-hologram rotation to remove the off-axis tilt in the reconstructed phase-contrast image. The Twyman-Green interferometer is employed with a microscope objective to investigate two objects: the first is a micro-lens array and the second is a step height. A hologram of the object is captured and then reconstructed to extract the wrapped phase map. The same hologram is rotated 180o and then reconstructed to extract the wrapped phase map. The wrapped phase maps extracted from the original hologram and its rotation 180o are unwrapped by the graph cuts algorithm and subtracted to produce a continuous phase-contrast image free from the off-axis tilt. The windowed Fourier filtering (WFF) method is applied to reduce the speckle noise in the continuous phase-contrast image to the slightest measure. Experimental results show that the off-axis tilt in the reconstructed phase-contrast image is completely removed. Moreover, the WFF's application significantly enhances the measurement profile.

Keywords: Digital holographic microscopy; 3D phase unwrapping; Optical metrology.

1. Introduction

Digital holographic microscopy (DHM) is used widely in many applications such as surface metrology and has been a powerful tool for label-free quantitative phase imaging. The merits of DHM are robust, precise, and physically non-contact [1-4]. DHM systems usually employ a microscope objective (MO) in the object arm to magnify the microstructures of the object being measured in the field of view. The reference arm of the interferometer may include identical MO or may not. The absence of MO in the reference arm may provide a good measurement since the

optical aberrations [5-9] are decreased. Moreover, it leads to system's non-complexity and the cost of the system, which is reduced. In off-axis digital holographic microscopy, the off-axis tilt is induced by the off-axis angle between the object wave (O) and the reference wave (R). The off-axis tilt may bring measurement errors; thus elimination of such tilt is necessary for accurate measurement. Various approaches have been proposed to compensate for the off-axis tilt. Such compensation approaches are based on the spectrum centering methods [10], which permit tilt correction by shifting the carrier frequency of the virtual image to the center of the hologram spectrum. The spectrum-centering judgment methods require prior knowledge of the system to extract the phase-contrast image in the spatial domain. Numerical fitting techniques [11] were employed to compensate for the off-axis tilt, however, such techniques need and rely on additional computational fitting procedures, which may sensitive to noise. In this paper, we used a compensation method based on hologram rotation to remove the off-axis tilt in the reconstructed phase-contrast image [12-13]. The off-axis tilt is completely removed by subtracting the rotated hologram's unwrapped phase from the original hologram's unwrapped phase. The whole process does not require prior knowledge of the system, additional fitting procedures, or complex spectrum centering judgment. The compensation method has been applied to reconstruct two objects with excellent results. The first object is a micro-lens array and the second object is a step height. Since the used light is relatively coherent and the surfaces of the measured samples are not perfectly smooth, speckle noise may arise [14-17]. Speckle noise debases the image quality and hence affects negatively the reconstructed phase-contrast image. The WFF has been used to reduce the speckle noise in the unwrapped phase-contrast image to the least measure [18-20]. The results of combining the compensation method with the WFF method prove that this combination can be used for accurate surface measurement.

2. Experiment

A typical Twyman-Green interferometer with a microscope objective in the object arm is depicted in Fig.1. The light source is a laser diode of a wavelength of 635 nm. A polarizer was mounted to tune the beam intensity. The beam was focused in a pinhole (diameter of 12.5 μm) through a focusing lens (10 mm focal length and 5 mm diameter). The outgoing beam from the pinhole passed through a collimating lens (100 mm focal length and 50 mm diameter) to generate parallel plane waves. A non-polarized beam-splitter (NPBS) divided the plane waves into two copies. One copy enters the reference arm of the interferometer, while the other copy enters the object arm of the interferometer via a microscope objective MO from Olympus (10x, NA = 0.30) to magnify the microstructures of the object being measured. The reference mirror was tilted to create a small angle between O and R. The reflected spherical light waves from the object interfere with the plane waves reflected from the reference mirror at the NPBS to form a parabolic hologram (see inset 2 in Fig. 1). A CCD sensor with 1024 x 768 square pixels of 4.65 μm in size was used to record the parabolic hologram via an imaging lens (3x, NA = 0.1). Note that inset 1 is suitable for an interference geometry with no MO in the object arm, while inset 2 in Fig. 1 is suitable for an interference geometry with the presence of two identical microscope objectives: one MO is placed

in the object arm and the other MO is placed in the reference arm. In preparation for measurement, all precautions have been taken to minimize systematic error [21].

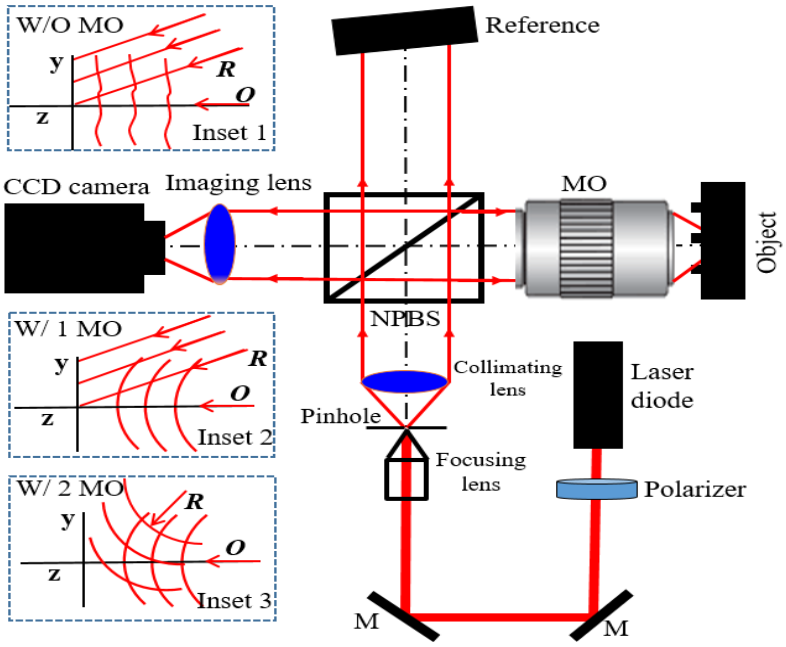

Fig. 1. Schematic diagram of the Twyman-Green interferometer with a microscope objective in the object arm. M; flat mirror, NPBS, non-polarizing beam splitter; MO1, and MO2, microscope objectives with (5x, NA = 0.13), (10x, NA = 0.30), respectively.

3. Reconstruction using the compensation method

Assume that the intensity of a digital hologram $I(x, y)$ is given by

$$I(x, y) = |O|^2 + |R|^2 + R^*O + RO^*, \qquad (1)$$

where x and y are discrete coordinates in the hologram plane, the first two intensity terms are of zero-order, which can be directly filtered in the Fourier domain, the last two are the interference terms, and * stands for the complex conjugate. The virtual image R*O combines a spherical wavefront, tilt, and a constant phase. It can be extracted from the I(x,y) by filtering its Fourier spectrum as

$$I_F(x, y) = R^*O = |O||R|\exp[i\varphi(x, y)]\tau(x, y), \qquad (2)$$

where $\varphi(x,y)$ is the phase of the object, $\tau(x,y)$ is the tilt which can be generally expressed as

$$\tau(x, y) = \exp\left(i(k_x x + k_y y)\right), \qquad (3)$$

where kx and ky are the linear phase difference between object wave O and reference wave R. Here, the off-axis tilt is compensated by the compensation method, which is based on a hologram rotation, while the spherical wavefront is compensated by the Zernike polynomials [22]. Suppose the original hologram with coordinate (x, y), the corresponding rotated hologram with coordinate (x', y'). The relation between the two coordinates can be written as

$$(x', y') = (x, y)\begin{bmatrix} -1 & 0 \\ 0 & -1 \end{bmatrix}. \qquad (4)$$

By using the Fourier transform, it's easy to know that the hologram is rotated 180o in the spatial domain; its Fourier spectrum will also rotate at the same angle in the frequency domain. It is clear that the +1 order of the original spectrum will rotate the same degrees and turn into the -1 order of the rotated hologram's spectrum. Therefore, the -1 order of the rotated hologram is given by

$$I_{RF}(x', y') = RO^{*} = |O||R|\exp[i\varphi(-x,-y)]\tau(-x,-y). \qquad (5)$$

Here, τ(-x,-y) = exp[i(- kx x - ky y)]. The off-axis tilt can be simply removed by subtracting the rotated hologram's unwrapped phase from the original hologram's unwrapped phase. The graph cuts algorithm was used to unwrap the wrapped phase map [23]. If the unwrapped phase of the original hologram is φ1 and the unwrapped phase of the rotated hologram is φ2, the difference in phase Φ between them is converted to height [10] as

$$h = \lambda(\Phi / 4\pi), \qquad (6)$$

where λ is the wavelength of illumination light. Since the used light is rather coherent and the surfaces of the measured samples are not exactly smooth, speckle noise may arise. Speckle noise debases the image quality and hence negatively affects the reconstructed phase-contrast image. The WFF has been used to reduce the speckle noise in the continuous phase-contrast image to the least measure. The hologram I (x, y) is convolved with the windowed Fourier transform (WFT) expressed as:

$$WFT(f_x, f_y) = \int_{-\infty-\infty}^{+\infty+\infty} I(x, y) r^{*}(x, y) dxdy, \qquad (7)$$

where r(x,y) = exp[-x2/200 −y2/200] is the Gaussian function and the symbol * denotes the complex conjugate operation. By shifting the central position of the Gaussian window point by point and computing the WFT of the signal, the fundamental spectral component of each local signal can be extracted. Then, by integrating all these spectral components, a universal spectral component can be retrieved as:

$$\int_{-\infty-\infty}^{+\infty+\infty} WFT(f_0, f_0) dxdy = F(f_0, f_0). \qquad (8)$$

Finally, applying the inverse Fourier transform to the universal spectral component, a complex image is obtained. The real values of the complex image have been taken to provide a speckle-free hologram. The obtained speckle-free hologram is then demodulated again by the compensation method to see the results with and without applying the WFF.

4. Results and discussions

4.1 Without the application of the WFF

The first object was investigated by the Twyman-Green interferometer, whose schematic diagram is shown in Fig. 1 is a micro-lens array (spherical Plano-convex microlenses with a lens diameter of 155 µm, lens pitch of 165 µm, and lens thickness of 16.5 µm [2]). The microscope objective MO with the imaging lens show only three microlenses in the field of view. The original hologram of the three microlenses is shown in Fig. 2(a). The rotated hologram with 180o is shown in Fig. 2(b). The 2D Fourier spectrum of Fig. 2(a) is shown in Fig. 2(c), while the 2D Fourier spectrum of Fig. 2(b) is shown in Figs. 2(d). As seen in Fig. 2(c) and Fig. 2(d), the tilt distribution of +1 order for original hologram is the same as that of -1 order for rotated hologram. The unwrapped phase map of the +1 order is shown in Fig. 3(a), while the unwrapped phase map of the -1 order is shown in Fig. 3(b). As seen in Fig. 3(a) and Fig. 3(b), without compensation, both unwrapped phase maps are affected by the tilt. Figure 3(c) shows the difference between Fig. 3(a) and Fig. 3(b). As seen in Fig. 3(c), the compensation method removes the off-axis tilt completely. The Zernike polynomials [22] corrected the parabolic curvature of Fig. 3(c). After correction, the phase map was converted to height map using Eq. 6 and the results are shown in Fig. 3(d).

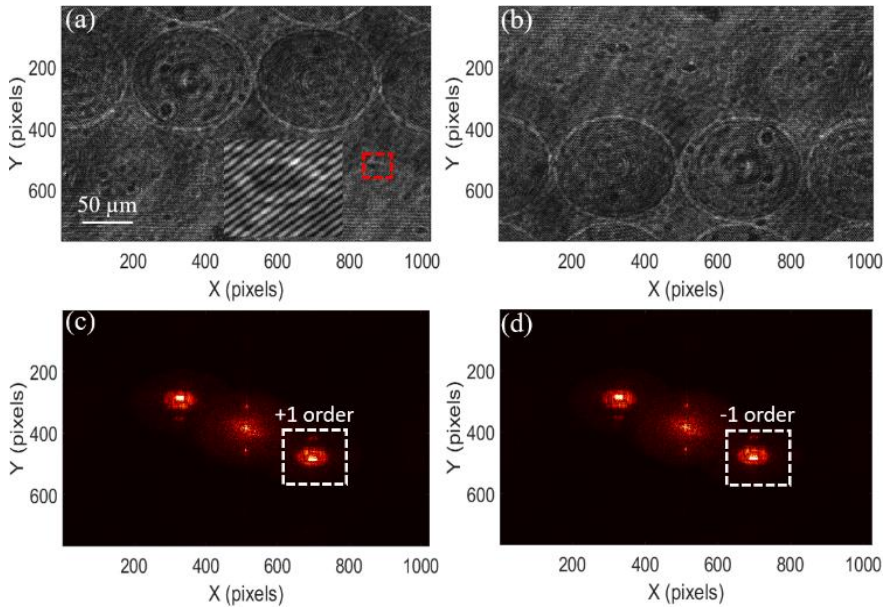

Fig. 2. (a) The micro-lens array hologram. (b) The rotated hologram of (a). (c) The 2D Fourier spectra of (a). (d) The 2D Fourier spectra of (b).

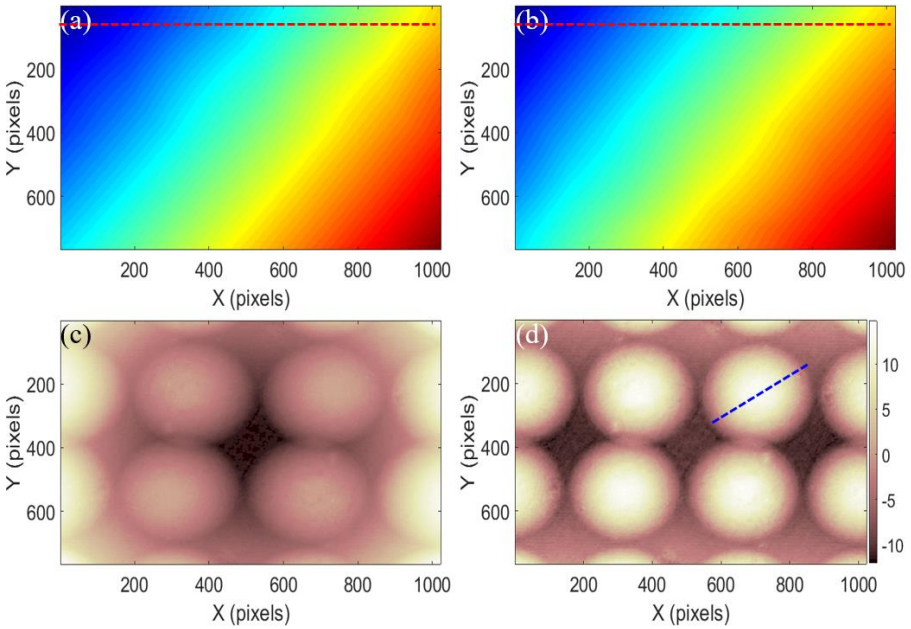

Fig. 3. (a) The unwrapped phase of the original hologram of Fig. 2(a) without tilt compensation. (b) The unwrapped phase of the rotating hologram of Fig. 2(b). (c) The difference between (a) and (b). (d) The correction (parabolic compensation) of (c). The unit of the color bar is in microns.

To show the performance of the compensation method in removing the off-axis tilt, the phase profiles along the red solid lines (red and blue colors) in Fig. 3(a) and Fig. 3(b) were given in Fig. 4(a). The difference between the two phase profiles produces a phase error (pink color) in Fig. 4(a), which is nearly zero, i.e. the off-axis tilt equals zero. The height profile along the dotted blue line of Fig. 3(d) is shown in Fig.4(b). The height profile is estimated to be in the range of 16.65 µm. The measured value is very close to the nominal value of 16.5 µm [2]. Note that, the compensation method was applied without the WFF method, so the profile of Fig. 4(b) is noisy.

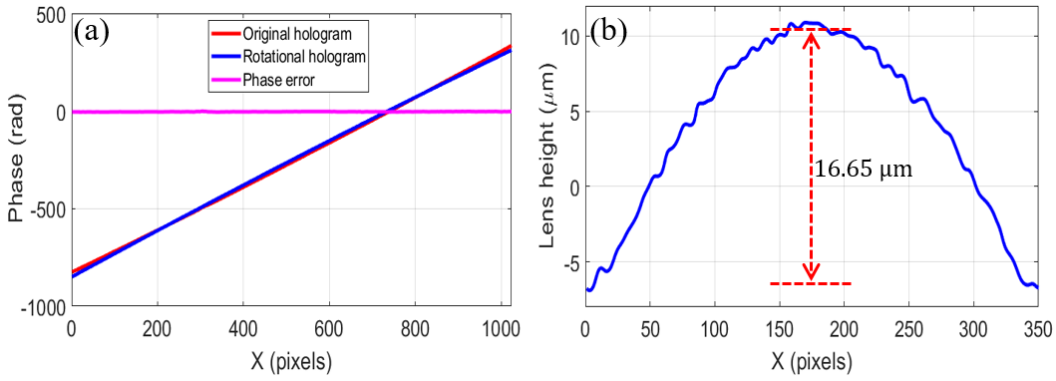

Fig. 4. (a) Phase profiles along the red solid lines in Fig. 3(a) and Fig. 3(b). (b) The height profile along the blue dotted line in Fig. 3(d).

The second object was investigated by the Twyman-Green interferometer, whose schematic diagram shown in Fig. 1 shows a step height of 1.34µm [10]. The original hologram of the step height is shown in Fig. 5(a). The rotated hologram with 180o is shown in Fig. 5(b). The 2D Fourier

spectra of Fig. 5(a) are shown in Fig. 5(c), while the 2D Fourier spectra of Fig. 5(b) are shown in Fig. 5(d).

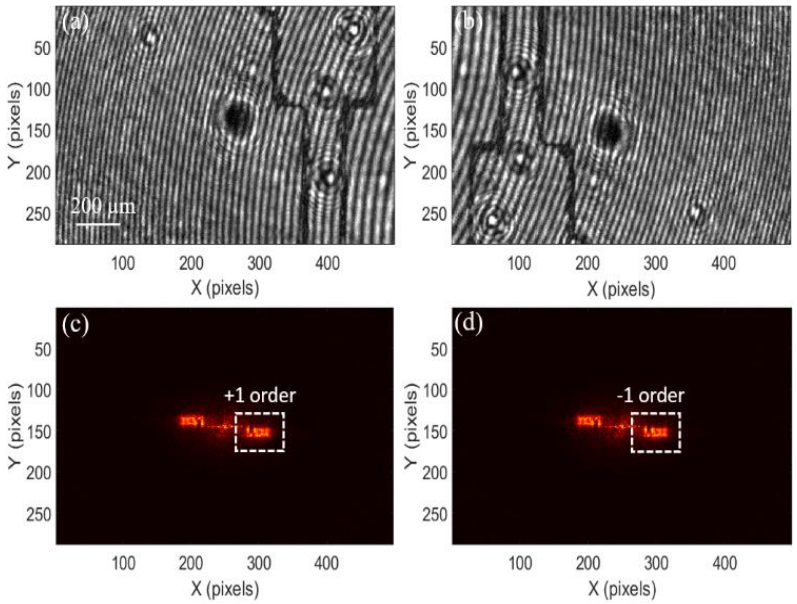

Fig. 5. (a) The step height hologram. (b) The rotated hologram of (a). (c) The 2D Fourier spectra of (a). (d) The 2D Fourier spectra of (b).

The unwrapped phase map of the +1 order is shown in Fig. 6(a), while the unwrapped phase map of the -1 order is shown in Fig. 6(b). Figure 6(c) shows the phase difference between Fig. 6(a) and Fig. 6(b). Figure 6(c) shows that the off-axis tilt is completely removed. The curvature of Fig. 6(c) was corrected by the Zernike polynomials [22]. The corrected phase map was converted to height map using Eq. 6 and the results are shown in Fig. 6(d).

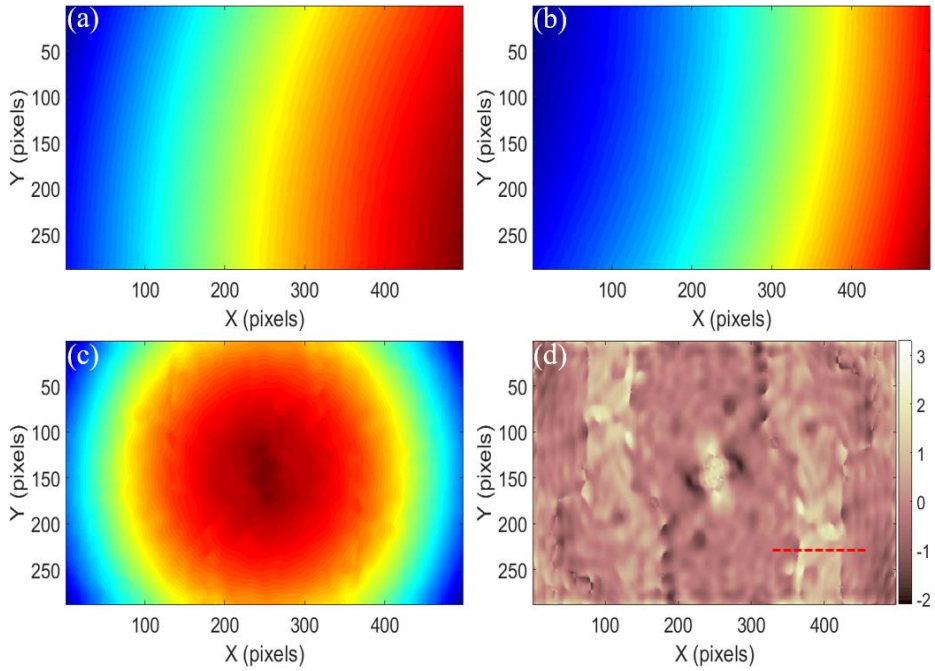

Fig. 6. The unwrapped phase of the original hologram of Fig. 5(a) without tilt compensation. (b) The unwrapped phase of the rotating hologram of Fig. 5(b). (d) The difference between (a) and (b). (d) The correction (parabolic compensation) of (c). The unit of the color bar is in microns.

The height profile along the dotted red line of Fig. 6(d) is shown in Fig.7. The height profile is estimated to be in the range of 1.39 µm. The measured value approaches the nominal value of 1.34 µm [10]. Since the profile looks noisy, we propose using the WFF to reduce the noise to the least measure.

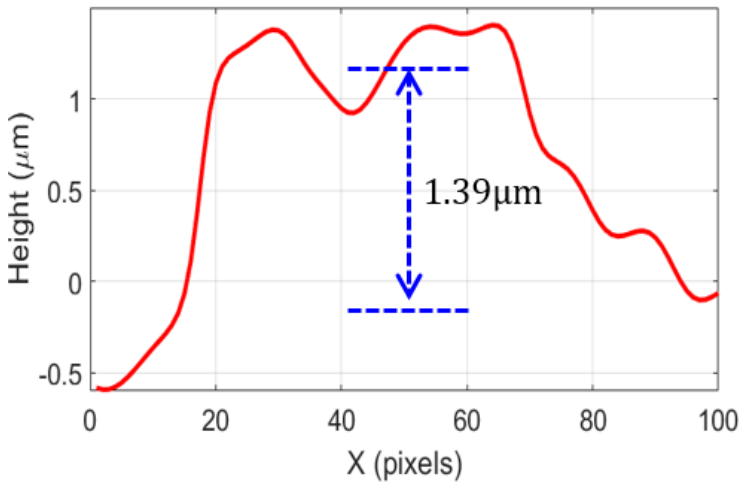

Fig. 7. The height profile along the red dotted line in Fig. 6(d).

4.2. With the application of the WFF

The original hologram is convolved first with the windowed Fourier transform (WFT) as in Eq. 7. By shifting the central position of the Gaussian window point by point and computing the WFT of the signal, the fundamental spectral component of each local signal is extracted. Integrating all the

spectral components can retrieve a universal spectral component as in Eq. 8. By applying the inverse Fourier transform to the universal spectral component, a complex image is obtained. The real values of the complex image have been taken to provide a speckle-free hologram. Regarding the micro-lens array object, Fig. 8(a) shows the enhanced hologram of Fig. 2(a) after applying the WFF method. Figure 8(b) shows the rotated hologram of Fig. 8(a). The 2D Fourier spectrum of Fig. 8(a) is shown in Fig. 8(c), while the 2D Fourier spectrum of Fig. 8(b) is shown in Figs. 8(d). The unwrapped phase map of the +1 order is shown in Fig. 9(a), while the unwrapped phase map of the -1 order is shown in Fig. 9(b). Figure 9(c) shows the difference between Fig. 9(a) and Fig. 9(b). Figure 9(d) shows the height map of Fig. 9(c) after correction with the Zernike polynomials [22] and conversion to the height map using Eq. 6. As seen in Fig. 9(c) and Fig. 9(d), the images are free from speckle noise thanks to the application of the WFF method. To confirm this point, a height profile along the dotted blue line of Fig. 9(d) was extracted as shown in Fig. 10 (a). The lens height profile was estimated to be in the range of 16.54 µm. The measured value of the lens height is enhanced and became very close to the nominal value, which is 16.5 µm [2]. The difference in height between the profiles in Fig. 4(b) and Fig. 10(a) is shown in Fig. 10(b). The root mean square (RMS) value of Fig. 10(b) is 0.4 µm.

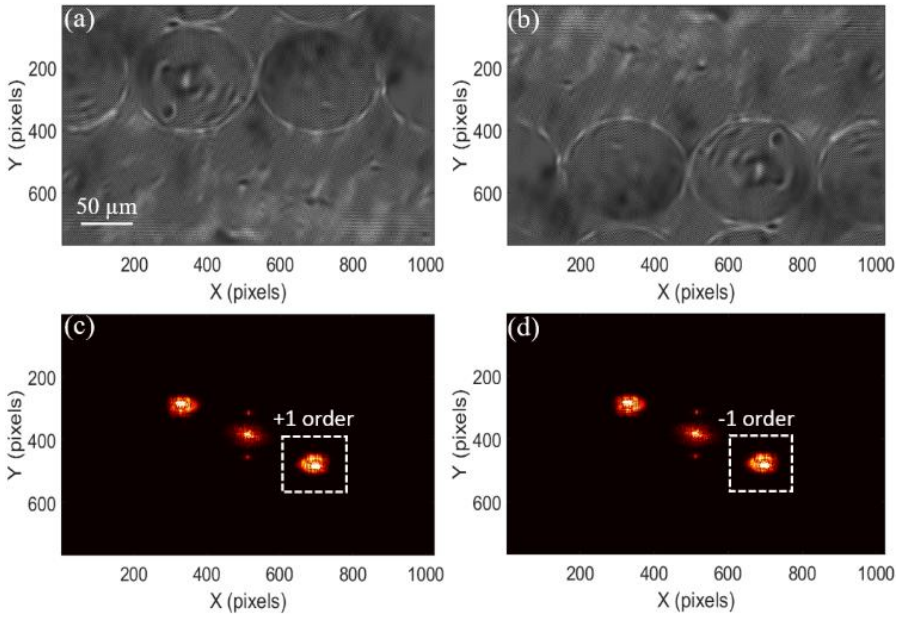

Fig. 8. (a) The micro-lens array of the enhanced hologram of Fig. 2(a) by the WFF method. (b) The rotated hologram of (a). (c) The 2D Fourier spectra of (a). (d) The 2D Fourier spectra of (b).

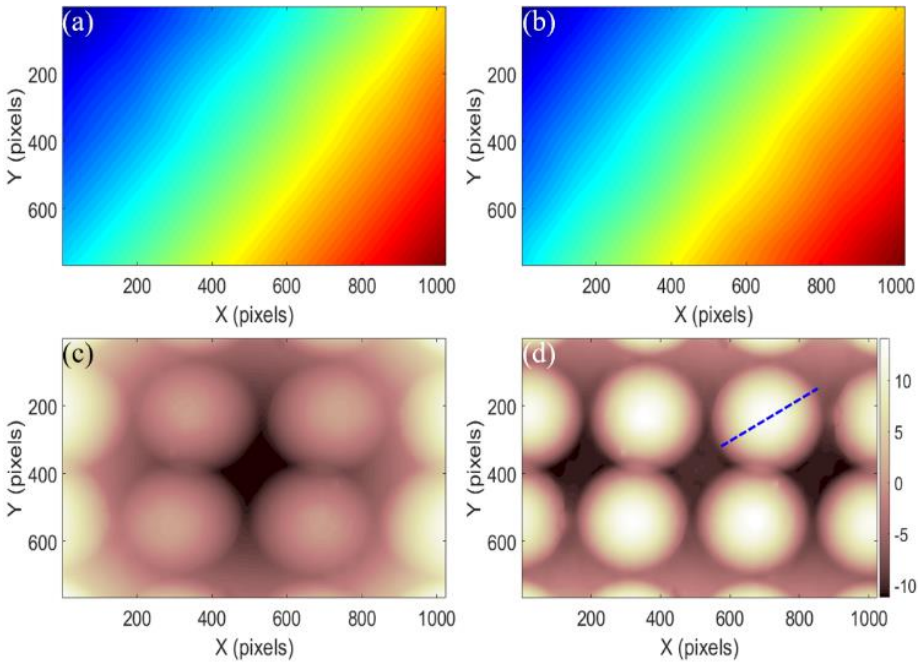

Fig. 9. (a) The unwrapped phase of the original hologram of Fig. 8(a) without tilt compensation. (b) The unwrapped phase of the rotating hologram of Fig. 8(b). (c) The difference between (a) and (b). (d) The correction (parabolic compensation) of (c). The unit of the color bar is in microns

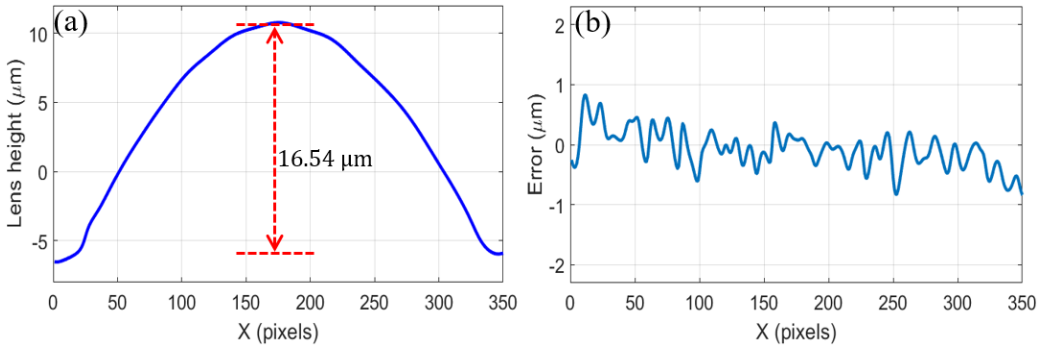

Fig. 10. (a) The height profile along the blue dotted line in Fig. 9(d). (b) The difference in height between the profiles in Fig. 4(b) and Fig. 10(a), the RMS is in the range of 0.4 μm.

Regarding the step height object, Fig. 11(a) shows the enhanced hologram of Fig. 5(a) after applying the WFF method. Figure 11(b) shows the rotated hologram of Fig. 11(a). The 2D Fourier spectrum of Fig. 11(a) is shown in Fig. 11(c), while the 2D Fourier spectrum of Fig. 11(b) is shown in Figs. 11(d). The unwrapped phase map of the +1 order is shown in Fig. 12(a), while the unwrapped phase map of the -1 order is shown in Fig. 12(b). Figure 12(c) shows the difference between Fig. 12(a) and Fig. 12(b). Figure 12(d) shows the height map of Fig. 12(c) after correction with the Zernike polynomials [22] and conversion to the height map using Eq. 6. As seen in Fig. 12(c) and Fig. 12(d), the images are free from speckle noise thanks to the application of the WFF method. To see it clearly, a height profile along the dotted red line of Fig. 12(d) was extracted as shown in Fig. 13 (a). The step height profile was estimated to be in the range of 1.34 μm. The measured value of the step height is enhanced and became consistent with the nominal value,

which is 1.34 µm [10]. The difference in height between the profiles in Fig. 7 and Fig. 13(a) is shown in Fig. 13(b). The root mean square (RMS) value of Fig. 13(b) is in the range of 0.14 µm.

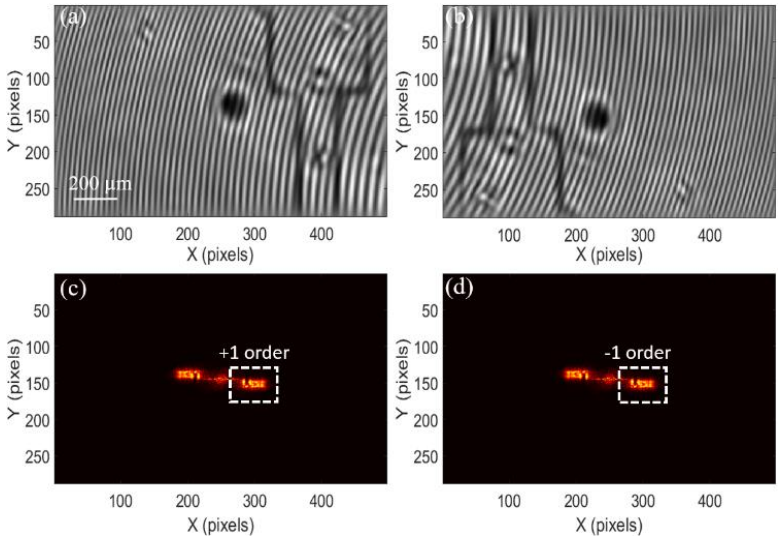

Fig. 11. (a) The step height of the enhanced hologram of Fig. 5(a) using the WFF method. (b) The rotated hologram of (a). (c) The 2D Fourier spectra of (a). (d) The 2D Fourier spectra of (b).

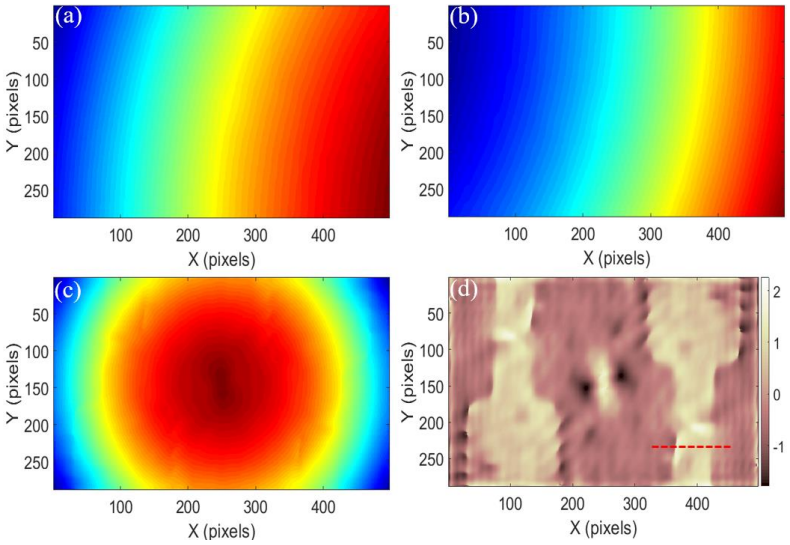

Fig. 12. The unwrapped phase of the enhanced hologram of Fig. 11(a) without tilt compensation. (b) The unwrapped phase of the rotating hologram of Fig.11(b). (d) The difference between (a) and (b). (d) The correction (parabolic compensation) of (c). The unit of the color bar is in microns.

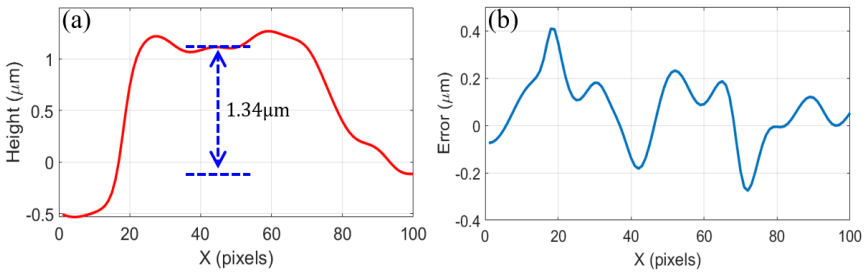

Fig. 13. (a) The height profile along the red dotted line in Fig. 12(d). (b) The difference in height between the profiles in Fig. 7 and Fig. 13(a), the RMS is in the range of 0.14 μm.

5. Conclusion

This work introduced a compensation method for off-axis tilt elimination in digital holographic microscopy. The method is based on subtracting the reconstructed continuous phase maps of the original hologram from its rotation 180o. Since the windowed Fourier filtering method significantly reduces the speckle noise, combining the compensation method with the windowed Fourier filtering was applied to reconstruct a micro-lens array and a step height with excellent results. The combination method is suitable for quantitative real-time phase imaging without prior knowledge, or complex spectrum-centering manipulations.

6. Declarations

6.1 Study Limitations

None.

6.2 Funding source

None.

6.3 Competing Interests

None.

References

1. Guo R. and Wang F. Compact and stable real-time dual-wavelength digital holographic microscopy with a long working distance objective, Optics Express, 25, 24512-24520 (2017).
2. Weijuan Q., Yingjie Y., Choo C. O., and Asundi A. Digital holographic microscopy with physical phase compensation, Optics Letters, 34, 1276 – 1278 (2009).
3. Abdelsalam D. G., Magnusson R., and Kim D. Single-shot, dual-wavelength digital holography based on polarizing separation, Applied Optics, 50, 3360-3368 (2011).
4. Gao P., Yao B., Min J., Guo R., Ma B., Zheng J., Lei M., Yan S., Dan D., and Ye T. Autofocusing of digital holographic microscopy based on off-axis illuminations, Optics Letters, 37, 3630–3632 (2012).
5. Abdelsalam D. G., Min J., Kim D., and Yao B. Digital holographic shape measurement using Fizeau microscopy, Chinese Optics Letters, 13, 100701-5 (2015).
6. Ferraro P., Nicola S. De, Finizio A., Coppola G., Grilli S., Magro C., and Pierattini G. Compensation of the inherent wavefront curvature in digital holographic coherent microscopy for quantitative phase-contrast imaging, Applied Optics, 42, 1938-1946 (2003).
7. Stadelmaier A. and Massig J. H. Compensation of lens aberrations in digital holography, Optics Letters, 25, 1630-1632 (2000).
8. Nicola S. De, Finizio A., Pierattini G., Alfieri D., Grilli S., Sansone L., and Ferraro P. Recovering correct phase information in multi-wavelength digital holographic microscopy by compensation for chromatic aberrations, Optics Letters, 30, 2706-2708 (2005).

9. Nicola S. De, Ferraro P., Finizio A., and Pierattini G. Wavefront reconstruction of Fresnel off-axis holograms with compensation of aberrations by means of phase-shifting digital holography, Optics and Lasers in Engineering, 37, 331-340 (2002).
10. Abdelsalam D. G. and Kim D. Real-time dual-wavelength digital holographic microscopy based on polarizing separation, Optics Communications, 285, 233-237 (2011).
11. Colomb T., Montfort F., Kühn J., Aspert N., Cuche E., Marian A., Charrière F., Bourquin S., Marquet P., and Depeursinge C. Numerical parametric lens for shifting, magnification, and complete aberration compensation in digital holographic microscopy, J. Opt. Soc. Amer. A, 23, 3177–3190 (2006).
12. Ibrahim D. G. A. Rough surface characterization using off-axis digital holographic microscopy compensated with self-hologram rotation, Current Applied Physics, 18, 1261-1267 (2018).
13. Deng D., Qu W., He W., Wu Y., Liu X., and Peng X. Off-axis tilt compensation in common-path digital holographic microscopy based on hologram rotation, Optics Letters, 42, 5282 – 5285 (2017).
14. Xiao-ou C. Reduction of speckle noise in the reconstructed image digital holography, Optik, 121, 394-399 (2010).
15. Ibrahim D. G. A. Optical Metrology with Interferometry, Cambridge Scholars Publishing, London, (2019).
16. Ibrahim D. G. A. Quantitative phase imaging using a combination of flat fielding and windowed Fourier filtering demodulated by a graph cuts algorithm for screening opaque and transparent objects, Optics Continuum, 1, 246-260 (2022).
17. Abdelsalam D. G., and Kim D. Coherent noise suppression in digital holography based on flat fielding with apodized apertures, Optics Express, 19, 17951-17959 (2011).
18. Kemao Q. Windowed Fourier transform for fringe pattern analysis, Applied Optics, 43, 2695-2702 (2004).
19. Kemao Q. Windowed Fourier transform method for demodulation of carrier fringes, Optical Engineering, 43, 1472-1473 (2004).
20. Kemao Q., Wang H., and Gao W. Windowed Fourier transform for fringe pattern analysis: Theoretical analyses, Applied Optics, 47, 5408- 5419 (2008).
21. Ibrahim D. G. A. Estimation of an uncertainty budget and performance measurement for a dual-wavelength Twyman-Green interferometer, Journal of Microscopy, 282, 224-238 (2021).
22. Abdelsalam D. G., Shaalan M. S., Eloker M. M., Kim D. Radius of curvature measurement of spherical smooth surfaces by multiple- beam interferometry in reflection, Optics and Lasers in Engineering, 48, 643-649 (2010).
23. Bioucas-Dias J. M., and Valadão G. Phase unwrapping via graph cuts, IEEE Trans. on Image Process. 16,698-709 (2007).